Journal of Applied Polymer Science

Synthesis and characterization of polyethylene/oxidized polyethylene miscible blends and role of OPE as a viscosity control

Muhammad Z. Iqbal,[1] Ahmed A. Abdala,[2,3] Matthew W. Liberatore[1]*

[1]Department of Chemical and Biological Engineering, Colorado School of Mines, Golden, CO 80401

[2]Materials Science and Engineering Division, Qatar Environment and Energy Research Institute, Hamad Bin Khalifa University, Doha, Qatar

[3]College of Sciences and Engineering, Hamad Bin Khalifa University, Doha, Qatar

Correspondence to: M. W. Liberatore (E-mail: matthew.liberatore@utoledo.edu)

*Present address: Department of Chemical and Environmental Engineering, University of Toledo, OH, 43606

ABSTRACT: Polymer blending allows for new materials to be designed with unique properties. Here, blends of linear low density polyethylene (PE) and oxidized polyethylene (OPE) have been prepared. PE/OPE blends are characterized for their molten state properties by thermal analysis and rheology; the solid state properties are studied by scattering, diffraction, and tensile testing. Melt miscibility was confirmed by a negative Flory-Huggins interaction parameter ($\chi \sim -2.3$) from Hoffman-Weeks plots. Additionally, a continuous decrease in melting temperature (from 123 to 119 °C) and thermal stability of blends (25% weight loss from 454 to 416 °C) was observed with increasing OPE loading from 0 to 50 wt %. Time-temperature master curves revealed the shifting of the glassy region to higher frequencies and formation of relaxed polymer chains in the glassy region. A plasticization effect was observed with zero shear viscosity of the blends decreasing with increasing OPE loading. Finally, a decrease in lamellar thickness of PE (from 180 to 140 Å) with increasing OPE resulted in increasing the blends' brittleness. © 2016 Wiley Periodicals, Inc. J. Appl. Polym. Sci. **2016**, *133*, 43521.

KEYWORDS: blends; mechanical properties; morphology; rheology; synthesis and processing

Received 9 November 2015; accepted 3 February 2016

DOI: 10.1002/app.43521

INTRODUCTION

Polymer blending is an economical way of designing new materials with unique properties, such as high impact strength by leveraging the interactions between similar and dissimilar polymer chains. The estimated consumption of polymer blends is more than 35% of the total polymer consumption around the world and is continuing to increase.[1] The properties of pure polymers are important in predicting the resultant blend properties. Therefore, generating new structure-property relationships between pure polymers and their blends can lead to new high performance materials.[1,2] In general, the bulk properties of blends depend on its phase morphology and interfacial structures.

Polymer blends are categorized as immiscible, miscible, or partially miscible. In immiscible blends, one polymer can form a discrete phase dispersed in the other polymer whereas in miscible blends, a single phase is observed. Also, partially miscible blend can exhibit a single phase or multiple phases.[3] Owing to the high molecular weight and small entropy of mixing, polymer blends usually exhibit immiscibility.[4] Examples of commercial immiscible blends include polystyrene with butadiene to produce high impact polystyrene[5] or poly(ethylene terephthalate) with poly(vinyl alcohol) for beverage bottles with better barrier properties.[6] Conversely, a small number of polymers shows miscibility when blended, such as polystyrene with poly(phenylene oxide),[7] poly (vinyl chloride) with polycaprolactone,[8] and poly(vinylidene fluoride) with poly(methyl methacrylate).[9,10] Usually, the miscibility is observed when mixing polymers leads to molecular ordering. For example, when polystyrene is blended with poly(phenylene oxide), the phenyl rings in both polymers overlap due to π-π interactions creating miscible blends.[7]

Polyolefins are used in packaging films,[11–15] but due to their nonpolar nature, exhibit poor printability and dye-ability.[16] Polyolefin blends with thermoplastics can create new materials that impart polarity in polyolefins by mixing, allowing for dispersing fillers, such as talc, carbon black, and graphene.[16] Introducing a small amount of polar groups onto the polymer backbone during polymerization[17] or via post-polymerization process[18] can overcome the nonpolar nature of polyolefins, but costs increase

Additional Supporting Information may be found in the online version of this article.

substantially. On the other hand, blending polyolefin, such as linear low density polyethylene (PE), with another polar polymer to prepare miscible blends can impart polarity in the blend matrix.

Oxidized polyethylene (OPE), commonly known as polymer wax, is often used as a processing aid[19,20] or biodegradable PE.[21] The OPE is synthesized by oxidizing PE by thermal,[22] radiation,[23] or chemical methods.[24] The oxidation process breaks the polymer chains into segments of small molecular weight while introducing polar groups (e.g., acidic and ester groups) at the chain ends and along the chains.[25,26] OPE is weaker and more brittle than PE, but when mixed with PE, it can ease processing by decreasing viscosity. Durmus *et al.*[25] used OPE as a compatibilizer in PE/clay nanocomposites and compared the properties of OPE compatibilized nanocomposites with conventional PE-grafted-maleic anhydride compatibilized nanocomposites. They reported ~120% reduction in oxygen permeability in the OPE compatibilized nanocomposites at 15 wt % OPE loading, which was attributed to increased exfoliation of clay. Also, OPE compatibilized nanocomposites improved barrier properties and lowered the clay aspect ratio.[27] Thus, PE/OPE blends show potential for packaging applications. However, a more detailed understanding of the interactions of OPE with PE is needed to engineer properties to create new products.

In this work, a comprehensive study of PE/OPE blends prepared by solution blending is reported. The miscibility of the blend was determined by the Flory-Huggins parameter. The rheological, mechanical, thermal and morphological properties of the blends were characterized. Finally, the molecular morphology was correlated with the macroscopic properties.

EXPERIMENTAL

Materials

Linear low density polyethylene (LLDPE) with molecular weight of 3.6×10^6 g/mol (determined via gel permeation chromatography) and bulk density of 0.97 g/cm^3 was purchased from Aldrich (428078, lot#07730MEV). Oxidized polyethylene (OPE) with an acid number of 7 and density of 0.94 g/cm^3 (molecular weight $\sim 1 \times 10^3$ g/mol) was supplied by Marcus Oil and Chemicals (Texas). The Newtonian viscosity of LLDPE at 160 °C is 1×10^4 Pa-s, and that of OPE at 145 °C is 0.02 Pa-s (viscosity versus temperature is provided in supporting information). The solvent p-xylene (purity ~ 99%, Sigma Aldrich, 134449) was used as received.

Preparation of Blends

PE and OPE at various compositions were dispersed in p-xylene (10 wt % solution) at 120 °C for two h. After the formation of homogenous and transparent solution, the solution was drop cast on a heated glass plate at 120 °C, and the solvent evaporated at that temperature for 2 h. The complete solvent removal was achieved by drying in a fume hood at ambient conditions for 24 h followed by drying for 5 h at 80 °C in a convection oven. The samples were further vacuum dried overnight. The complete solvent removal was confirmed by running thermal scans in a differential scanning calorimeter where no solvent evaporation peak was observed. The dried samples were cut into pieces 3-5 mm wide, heated at 160 °C for 10 min and hot pressed for 3 min under 5000 kPa pressure to prepare circular discs (thickness $\sim 1-1.3$ mm and diameter ~ 25 mm) for rheological testing. Similarly, thin films ($100-200$ μm) were prepared for mechanical and scattering testing by the same method using more dilute solutions of PE and OPE in p-xylene and drop casting in a petri dish at 120 °C and following the same drying process.

Characterization

The thermal transitions of the blends were investigated using DSC (TA Instruments Q20). About 5-10 mg sample was heated under nitrogen flow (20 mL/min) at 10 °C/min from RT to 160 °C, isothermally heated for 3 min to remove any previous thermal history, and cooled at 10 °C/min to room temperature in order to record the crystallization temperature, T_c. The melting temperature, T_m was determined from the second heating ramp at 10 °C/min from room temperature to 160 °C. For the determination of equilibrium melting point, after removing thermal history, the sample was rapidly cooled to a fixed T_c at a rapid rate of 60 °C/min to avoid premature crystallization, kept at T_c for 30 min, cooled to room temperature at 10 °C/min, and finally heated above the melting point at 10 °C/min to record the apparent melting associated with each T_c.

Thermal stability of the blends was determined by, TGA (TA Instruments Q50). Approximately, 10-20 mg of the sample was loaded in TGA sampling pan, heated from room temperature to 650 °C at 20 °C/min under nitrogen flow (60 mL/min).

The rheological properties of the pure and blend samples were studied using TA Instruments AR-G2 rheometer equipped with a 20 mm parallel plate. Time sweeps were conducted at 160 °C at 1% strain and 1 rad/s angular frequency. For time sweep, the samples were carefully loaded so that less than 80 s elapsed before data collection began. Samples were equilibrated at 180 °C for 2 min followed by 5 seconds at 160 °C under static conditions, pressed between the plates. The blends were subjected to time sweep experiments for 60 min. The linear viscoelastic region was determined by running stress sweep at each temperature at 1 Hz. The time-temperature superimposed master curves were constructed by conducting frequency sweeps at each temperature within the linear viscoelastic range using the horizontal shift factors.

The mechanical properties of blend films were determined following ASTM D882, using ARES-G2 (TA) extensional rheometer with Film & Fiber tool. Measurements were carried at room temperature under a speed of 0.0167 mm/s using thin rectangular samples ~10 mm long and ~5 mm wide, stretched at 0.166 mm/s^{-1} at room temperature. The reported mechanical properties are the average of 5 samples.

Small angle X-ray scattering (SAXS) and wide angle X-ray scattering (WAXS) experiments were performed at the X-ray Sciences Division, beamline 12-ID-B, at the Advanced Photon Source at Argonne National Laboratory. Details of the measurement procedure and the temperature and humidity control can be found elsewhere.[28,29] Wide angle X-ray diffraction (XRD) was performed using a Phillips PW 3040/60 spectrometer using

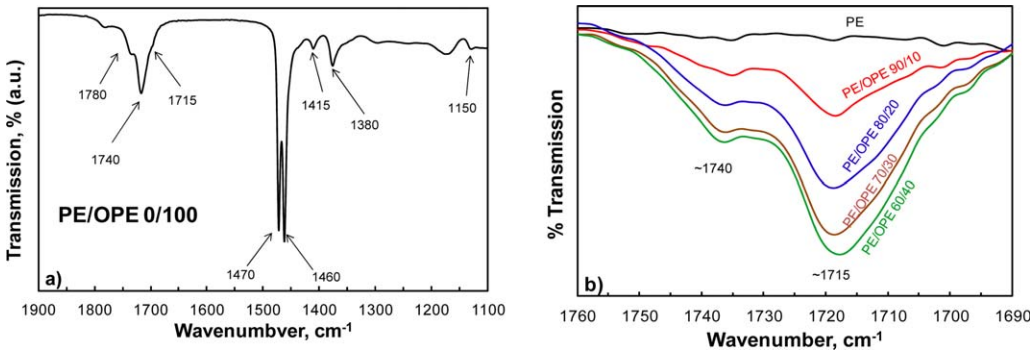

Figure 1. FTIR spectra of OPE (a) and PE/OPE blends at various compositions. [Color figure can be viewed in the online issue, which is available at wileyonlinelibrary.com.]

CuKα radiation at a scan rate of 0.02 °C/s. The samples for SAXS, WAXS, and XRD were prepared following procedure similar to that used for mechanical testing samples.

Fourier Transformed infrared (FTIR) spectra (32 scans at 4 cm^{-1} resolution) were collected using a Nicolet FTIR with ATR. The FTIR spectra were taken from 5 different spots on thin films and averaged.

The micro-images of the blends were obtained using JEOL-JSM-7000F field emission scanning electron microscope (FE-SEM) at an accelerating voltage of 3 KV. The blends were cryo-fractured in liquid nitrogen and spur coated with gold for 1-1.5 min.

RESULTS AND DISCUSSION

Miscibility, Phase Behavior, and Thermal Properties

Monitoring chemical bonds via FTIR spectroscopy provided the first qualitiative measure of the interactions between PE and OPE. Neat OPE showed specific vibrations originating from various O-containing groups [Figure 1(a)]. In the carbonyl range ($1600-1800$ cm^{-1}), symmetrical C═O stretching was observed at $\sim 1715-1780$ cm^{-1}, including the ketonic stretching at 1715 cm^{-1}, C═O stretch in esters at ~1740 cm^{-1}, and carboxylic acid C═O stretch at ~1780 cm^{-1}. The region in the frequency range of $1400-1500$ cm^{-1} was attributed to the combination of symmetric carboxylate stretch and C—H mode.[30] CH_2- stretching was observed at 1470 and 1460 cm^{-1}. C—H rocking absorption appeared at 1380 cm^{-1} and C—O stretch in tertiary alcohols observed at ~1150 cm^{-1}. Thus, OPE structure contained carbonyl C═O and ketonic C═O along with alcoholic C—O groups. The spectral regions of OPE were consistent with the structure of OPE reported elsewhere.[25]

The spectra of neat PE and PE/OPE blends were also obtained at various compositions [Figure 1(b)]. Since neat PE does not contain oxygen, no change in transmission was observed in the carbonyl region. Increasing the OPE concentration decreased the IR-transmission through the carbonyl peaks (at 1715 and 1740 cm^{-1}) in the blends, which is consistent with the location of the OPE functional groups. Averaging over 5 spots across the films, no changes in spectral patterns were observed, so the distribution of OPE within PE matrix appeared homogeneous.

Thermal properties of polymer blends describe application behavior of blends. Increasing OPE decreased the melting point and melt enthalpy of the blends (Figure 2). The melting temperature decreased from 123 °C for pure PE to 119 °C for 50/50 blend whereas there was no pattern observed for the melt enthalpy (ΔH_{exp}). ΔH_{exp} was in the range of 99 J/g for neat PE to 111 J/g for 50/50 blends. The melting profile of OPE showed three consecutive melting transitions in the range of 98–105 °C indicating presence of low molecular weight fractions in the commercial OPE samples, and ΔH_{exp} for OPE was 75 J/g (see supporting information). In addition, the crystallization temperature, and crystallization enthalpy are also provided in supporting information.

The melting profile for neat PE exhibited a peak melting point of 123 °C. As OPE was added into PE, a small shoulder appeared in the vicinity of PE's melting peak. Since this shoulder was less prominent in neat PE, the immiscible adsorption of OPE chains containing functional groups onto PE might be inferred. The small shoulder in PE melting profile indicated significant short chain branches that crystallize separately from the backbone of PE. The small separation between two melting peaks in neat PE was an indication that some chains do co-

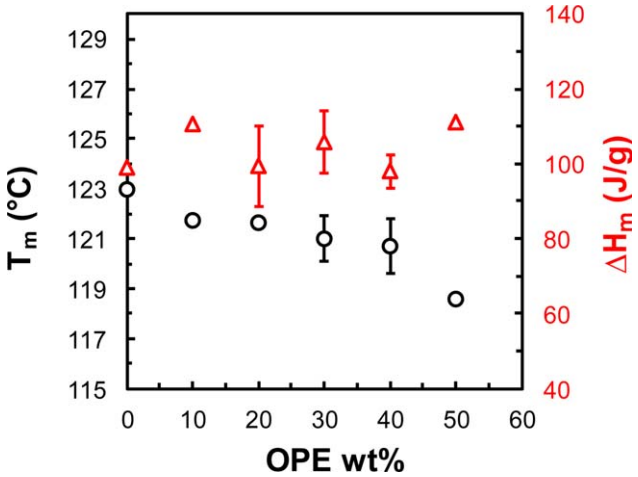

Figure 2. Melting temperature and melt enthalpy of the blends. [Color figure can be viewed in the online issue, which is available at wileyonlinelibrary.com.]

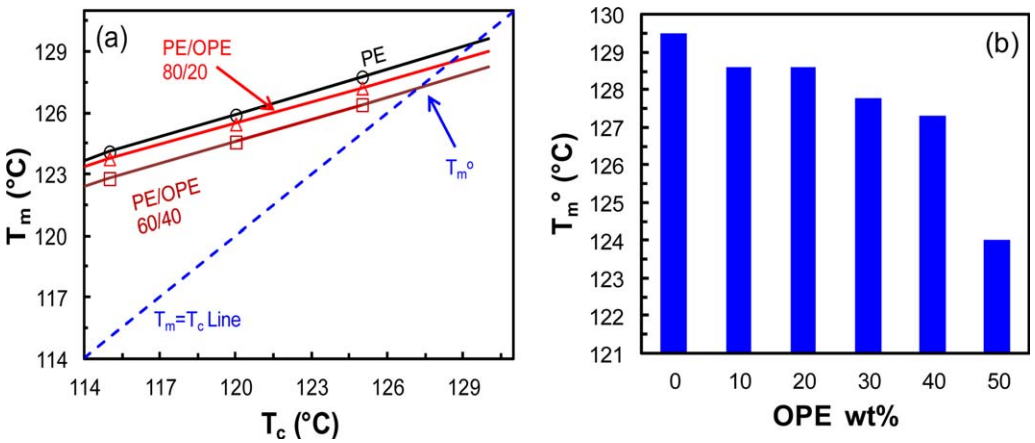

Figure 3. Hoffman-Weeks plot of PE/OPE blends (a) and T_m°: T versus OPE concentration (b). [Color figure can be viewed in the online issue, which is available at wileyonlinelibrary.com.]

crystallize.[13] Some of the OPE chains when blended with PE acted as diluents whereas the part that did not mix completely in PE might create the shoulder near the melting peak of PE. The shoulder increased with increasing OPE concentration in the blends whereas the melting peak of PE decreased as OPE concentration increased (supporting information). Due to the small separation between PE and the shoulder component, it is reasonable to believe the formation of single endotherm, which is indication of the miscibility between PE and OPE.[31]

Furthermore, the percent crystallinity in PE varied significantly increased with increasing the OPE loading. The percent bulk crystallinity was calculated by considering the enthalpy of melting of a 100% crystalline PE (ΔH°_{PE}) to be 293 J/g[32] by the formula crystallinity% = $\Delta H_{exp}/(\Delta H^\circ_{PE}$ x $\varphi_{PE})$ x 100. The measured bulk crystallinity% was 34, 42, 42, 52, 56, and 76% (±2%) for PE/OPE 100/0, 90/10, 80/20, 70/30, 60/40, and 50/50 blends, respectively. The significant increase in crystallinity also indicates formation of high modulus materials.

The χ-parameter has been evaluated experimentally using melting point depression following Hoffman-Weeks analysis (Figure 3) and Flory-Huggins theory (Figure 4). The Hoffman-Weeks equation[33] serves as the fundamental method of evaluating the equilibrium melting temperature (T_m°). The theory assumes that (1) surface effects in formation of crystals are negligible, (2) crystals at melting point exhibit equilibrium crystal perfections, and (3) the crystal thickening is independent of the crystallization temperature. The Hoffman-Weeks equation is expressed as:

$$T_m = T_m^\circ\left(1-\frac{1}{\gamma}\right)+\frac{T_c}{\gamma}$$

The observed melting temperature (T_m) was measured after isothermal crystallization at various crystallization temperatures (T_c). A plot between T_m and T_c gives a line and the point where the line intersects the $T_m = T_c$ line, gives T_m° for each blend composition. In the above equation, γ is the thickening coefficient equal to $l_c/l_g^\star$ where l_c is the thickness of grown crystal and $l_g^\star$ is the initial thickness of a chain-folded lamellar crystal.[33] The T_m° of neat PE and in blends was determined [Figure 3(a)]. A decrease in T_m° of PE was observed with increasing OPE concentration in PE/OPE blends, an indication of the miscibility.[9,34] The T_m° decreased from 129 °C for pure PE to 124 °C for the 50/50 blend [Figure 3(b)]. The decrease in T_m° is caused by the morphological and thermodynamic effects. In terms of the thermodynamic effects, OPE acted as a miscible diluent that decreased the chemical potential of a crystalline polymer, which in turn decreased T_m° value.[34,35]

Thermodynamically, the chemical potential of a crystallizable polymer decreases with addition of miscible diluents.[34] The decrease in chemical potential leads to reduction in T_m°, which is caused by the morphological and thermodynamic effects. Considering only the thermodynamic effects for T_m° depression, the Flory-Huggins theory[36] modified by Nishi-Wang[9] can be used to determine the Flory-Huggins interaction parameter, χ as follows:

$$\left(\frac{1}{T^\circ_{m(pure)}}-\frac{1}{T^\circ_{m(blend)}}\right)=-\frac{R}{\Delta H^\circ}\frac{V_2}{V_1}\left[\frac{\ln\phi_2}{m_2}+\left(\frac{1}{m_2}-\frac{1}{m_1}\right)\phi_1+\chi\phi_1{}^2\right]$$

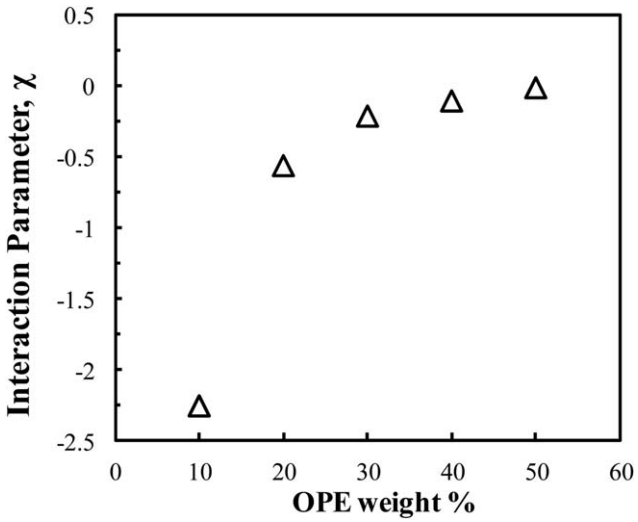

Figure 4. Composition dependence of the Flory-Huggins interaction parameter, χ.

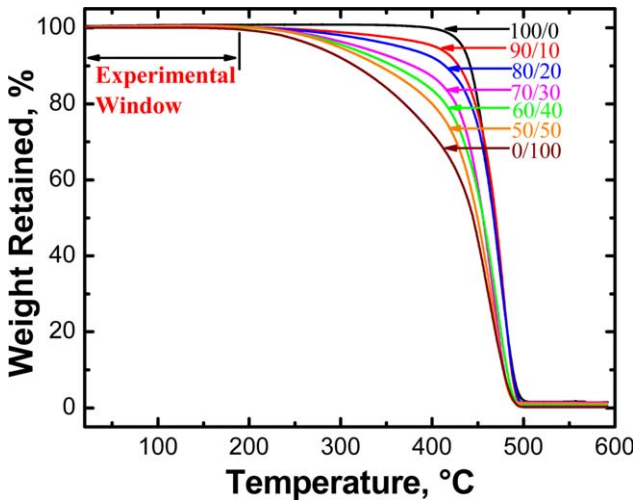

Figure 5. Thermal stability of PE/OPE blends. [Color figure can be viewed in the online issue, which is available at wileyonlinelibrary.com.]

Here, the subscripts 1 and 2 refer to OPE and PE, respectively. $T^{\circ}_{m(\text{pure})}$ and $T^{\circ}_{m(\text{blend})}$ are the equilibrium melting points of neat PE and that of PE in the blends, respectively. V_1 and V_2 are the molar volumes of the repeating units of the components, R is universal gas constant, ΔH° is the heat of fusion of a perfectly crystallizable polymer, m_1 and m_2 are the degrees of polymerization, ϕ is the volume fraction of the OPE in the blend and χ is the polymer-polymer interaction parameter (Flory-Huggins interaction parameter).

The ΔH° value for PE is 7870 J/mol.[37] Molar volumes of PE and OPE repeat units were calculated by the group contribution method.[38] The calculated molar volume of PE is $V_1 = 32.2$ cm^3/mol. The molar volume of OPE was calculated based on the structure reported by Durmus *et al.*[25] where OPE structure contained ketonic and carboxylic groups. For calculating the molar volume, two CH_2- groups, one ketonic group (-CO-) and one -O- group were considered whereas the end carboxylic functional groups (-COOH) were ignored. Thus, V_2 was calculated to be 46.8 cm^3/mol. Since both the components are polymers with large values of m_1 and m_2, these terms containing "m" can be neglected. Thus, the simplified version of the Flory-Huggins theory is:

$$\frac{\Delta H^{\circ}}{R}\frac{V_1}{V_2}\left(\frac{1}{T^{\circ}_{m(blend)}}-\frac{1}{T^{\circ}_{m(pure)}}\right)=\chi\phi_1{}^2$$

A plot between the left hand side of the above equation and $(1-\phi_2)^2$ should give a line with an intercept of zero, whereas the χ can be obtained from the slope of the line. The χ obtained, thus, is a single value, averaged over all the compositions. However, a critical analysis of above equation by Rostami[39] shows that this χ is actually composition dependent (Figure 4). A highly negative value of χ indicated miscibility which decreased as OPE concentration increased in the blends. Specifically, PE/OPE 90/10 exhibited $\chi = -2.3$ that jumped to -0.6 for 80/20 composition, and was $\sim$0 for 50/50 blend. The composition dependent χ has also been found for polyacrylamide-

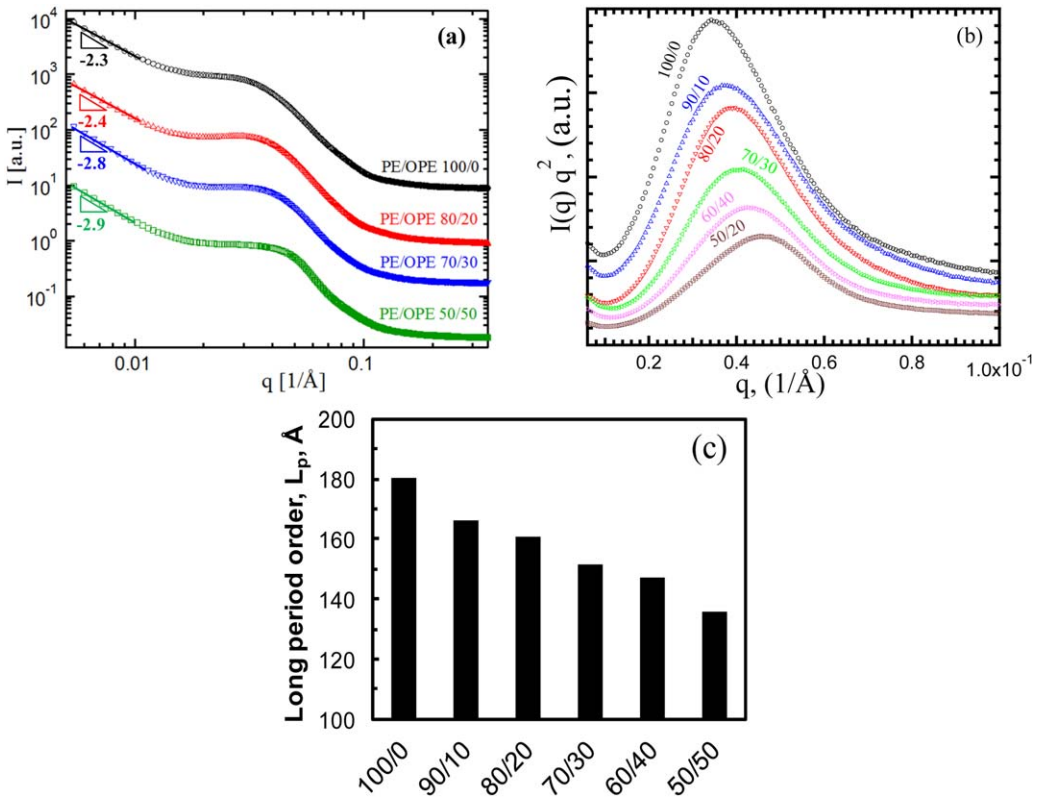

Figure 6. log-log I vs q (a) and Kratky plots of PE/OPE blends (b) at 60 °C and 0% relative humidity with Y-offset, and long period order for blends (c). [Color figure can be viewed in the online issue, which is available at wileyonlinelibrary.com.]

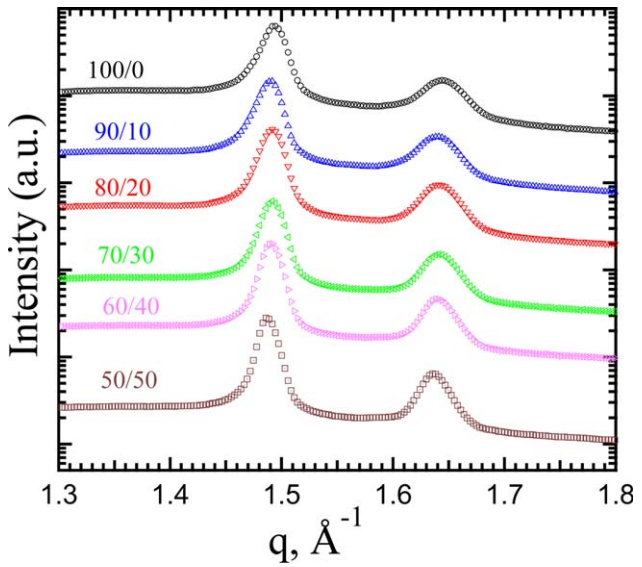

Figure 7. WAXS patterns of PE/OPE blends with Y-offset. [Color figure can be viewed in the online issue, which is available at wileyonlinelibrary.com.]

poly(ethylene glycol) system[34] and the blends of poly(ethylene oxide) with different polymers.[40] Moreover, a negative value of χ indicates miscibility[38] whereas positive χ shows incompatible blends.

The pure PE showed a high thermal stability, losses 25% weight at 454 °C, and decomposes completely at 500 °C. However, pure OPE exhibited low thermal stability, with weight loss starting around 200 °C, 25% weight loss by 389 °C, and complete decomposition at 490 °C. The thermal stability of the blend decreased with the inclusion of OPE (Figure 5). Since miscibility produces blends with properties in between the two pure components, the thermal stability of PE/OPE blends was in between that of neat PE and OPE. Due to the lower thermal stability of OPE, the blends started losing weight at about 200 °C and limited the experimental window for the rheological measurements. Therefore, the TTS master curves were constructed from 130 °C (~10 °C above the melting point) to 180 °C.

In addition, SAXS and WAXS explored the effect of OPE inclusion on PE structure. SAXS measures the shape and size of polymers between 5 and 25 nm of the repeat distances.[41] The scattering vector (q) probes different structural features at various length scales (length scale ~ $2\pi/q$) in a polymer. Increase in power law decaying exponent [$\log(I) \sim \log(q)^{-\alpha}$] at lower q indicates a larger size of scattering objects. A power law decaying exponent of $\alpha = 2.3$ for neat PE [Figure 6(a)] indicated the presence of randomly branched ideal polymer chains in PE.[42] Increasing exponent reflect the scattering from the mass fractals in polymers. A small increase of exponent to $\alpha = 2.4$ for 80/20 blend showed a slight increase in mass fractals in blends, whereas an exponent of $\alpha = 2.8$ for 70/30 compositions indicated a transition of morphology from ideal polymer chains to larger mass fractals.[43] A maximum exponent of 2.9 was observed for 50/50 blend, which showed stabilization of morphology between 30 and 50% OPE concentration.

The Kratky-SAXS profiles (also known as Lorentzian corrected plots) of the PE/OPE blends showed a maxima in the low q region [Figure 6(b)]. This maxima is associated with the periodicity resulting from the presence of macro-lattices formed by the centers of adjacent lamellae.[44] The arrangement of molecular chains in folded, unfolded, or partially unfolded lamellae can also be obtained from a Kratky profile.[45] Here, the long period, also called as weight-average value of the long period, L_p, was calculated from the maxima intensity peak in the Kratky plot. L_p decreased substantially from 180 Å for neat PE to 136 Å for 50/50 blends. The decrease in L_p is also attributed to the increase in microcrystallinity in the PE/OPE blends as confirmed by thermal analysis. This effect is further discussed in the mechanical properties section.

PE showed two distinctive peaks in the high q-range in WAXS profile at 1.49 $Å^{-1}$ and 1.64 $Å^{-1}$ (Figure 7). The small domain size (called d-spacing hereafter) associated with these peaks was calculated from $d = 2\pi/q$. A d-spacing of 4.2 Å and 3.8 Å for peaks were calculated. Interestingly, the inclusion of OPE in PE did not change the d-spacing in blends, and the blends exhibited a constant peak ratio of 1.1 across all compositions. Since, it was not possible to perform WAXS on OPE because it does not form a film at its own, the crystal structure of OPE was

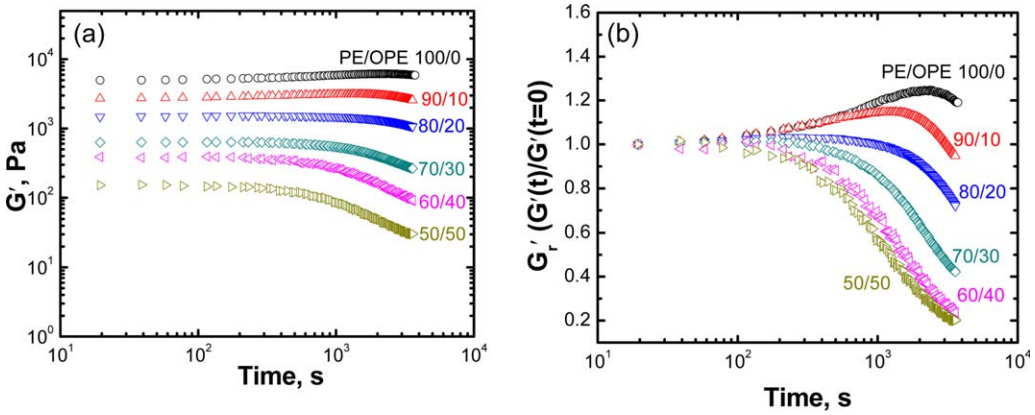

Figure 8. Start-up transient rheology of neat PE and PE/OPE blends: Evolution of G' with time (a), and reduced G' versus time. Data reported at $T = 160$ °C, $\gamma = 1\%$, $\omega = 1$ rad/s. [Color figure can be viewed in the online issue, which is available at wileyonlinelibrary.com.]

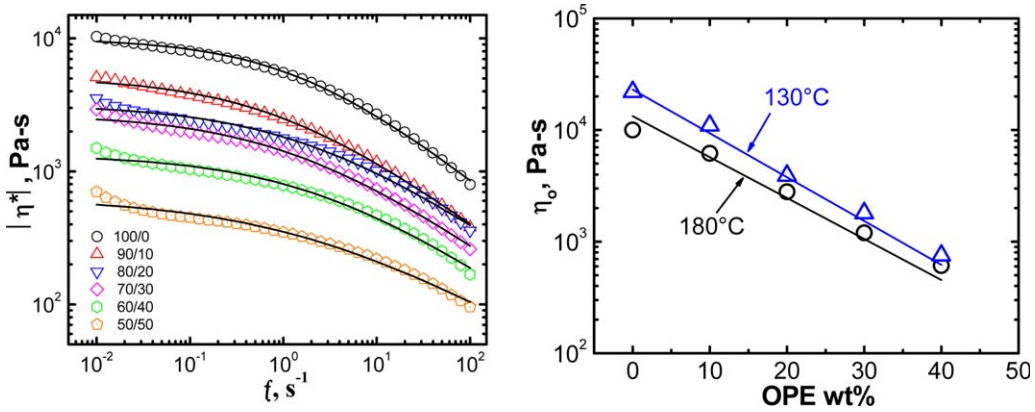

Figure 9. Complex viscosity profiles of PE/OPE blends at 160 °C. The black solid lines are the Cross model fit (left panel) and zero shear viscosity as a function of OPE wt % at two different temperatures (right panel). [Color figure can be viewed in the online issue, which is available at wileyonlinelibrary.com.]

obtained through X-ray diffraction (XRD) (supporting information). The PE/OPE blends exhibited almost similar XRD patterns as were observed in neat OPE or PE (also observed in WAXS). A nearly constant positions of crystalline peaks, and *d*-spacing indicates that the PE and OPE crystals are not different from each other, and the possibility of co-crystallization of PE and OPE. Further studies on the co-crystallization behavior of PE/OPE blends under isothermal and nonisothermal conditions could identify the nature and type of the formed crystals, but is outside the scope of this work.

Based on thermal and scattering results discussed above, the structure of PE and PE/OPE blends can be summarized as follows. PE consisted of lamellar structure containing the long period order of ~180 Å for neat PE, which reduced to ~136 Å at 50 wt % OPE loading. The substantial decrease in long period is directly associated with the increase in crystallinity of PE with OPE addition. The size of crystalline regions within the crystallites (*d*-spacing) remained unchanged, which indicates that OPE chains could be crystallizing with PE to produce similar crystals. Since, no quantitative argument could be made about the change in crystal size from WAXS, the increased crystallinity indicates that both amorphous and crystalline fractions of the long period are affected with OPE addition. This compact structure should exhibit higher modulus and increased brittleness compared to neat PE, which will be discussed in the mechanical properties section.

Melt Rheological Analysis

One important factor in designing new polymer blends is understanding their processing properties. Melt rheology is one of the most useful techniques to assess the processing behavior of polymers in the molten state to mimic the real time processing issues. Herein, time-dependent rheological properties were measured to understand the blends' thermal stability under processing conditions and time-temperature master curves were constructed to observe the chain dynamics over extended time scales.

The evolution of start-up transient rheological parameters is a common practice to understand thermal stability of polymers. Here, the evolution of G' was monitored with time at 160 °C at constant frequency and strain. A slight increase in G' was observed with time for neat PE [Figure 8(a)]. The 90/10 and 80/20 PE/OPE blends showed a similar small increase up to ~1000 s followed by a small level of thinning. At higher OPE concentration, the blends exhibited a stronger thinning starting below 1000 s. The thinning effect was more pronounced when reduced shear modulus, G_r' [where $G_r'=G'(t)/G'(t=0)$] was plotted against time [Figure 8(b)]. Neat PE showed about 20% increase in G_r' and the increment decreased for 90/10 blend followed by pure thixotropy with increasing OPE concentration in the blends. Thus, OPE acted as a plasticizer. The critical time (time at which rheological properties such as G', G'', and η^* drop significantly) decreased with increasing OPE concentration in blends. The power law exponent was evaluated as $G' \sim t^{\beta}$ where G' was considered in the thinning regions only. The evaluated shear thinning exponent, β, values were −0.18, −0.30, −0.38, −0.55, −0.82, −0.85 for 100/0, 90/10, 80/20, 70/30, 60/40 and 50/50 blends, respectively. As β increased, the blends showed a stronger shear thinning behavior. In subsequent sections, all samples were equilibrated at 180 °C for 2 min followed by equilibrating for 1 min at a specific temperature before carrying out any measurement. The experiments were completed within 350 s at all temperatures before the overshoot or shear thinning exceeded more than ±15%.

The plasticization effect of OPE on PE is more evident in Figure 9(a). Significant decrease in complex viscosity was observed with increasing OPE amount. For example, neat PE showed a viscosity of 10,000 Pa-s (at 0.01 Hz) that was reduced by more than one order of magnitude to 700 Pa-s for 50/50 blend.

The zero shear viscosity (η_0) of the blends at various temperatures is determined by fitting the complex viscosity data with Cross model,[46] which will be compared next.

$$\eta(\omega)=\frac{\eta_0}{\left[1+(\tau_o\omega)^{1-n}\right]}$$

Where, η_0 is the zero shear viscosity, τ_0 is the relaxation time related to the longest relaxation time and n is the Cross-exponent. The Cross fitting parameters and fitting profiles are given in the supporting information.

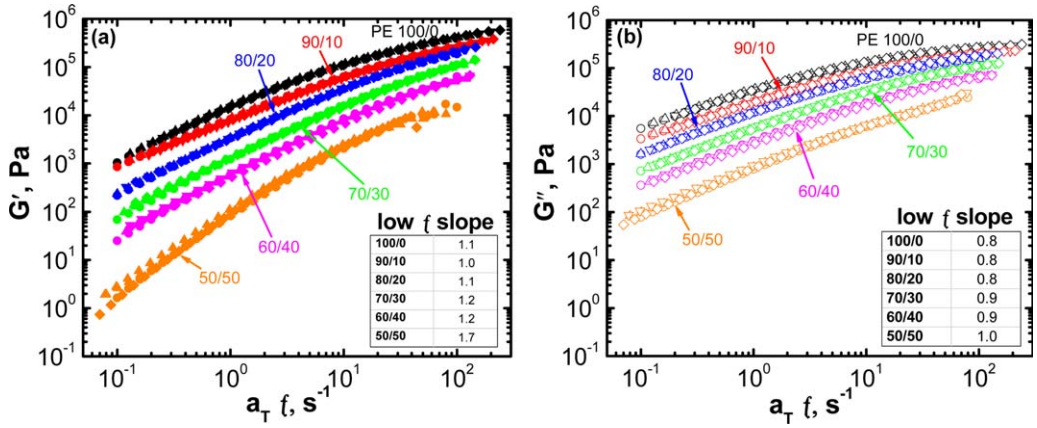

Figure 10. Master curves for G' (a), G'' (b) over the reduced frequency. Insets in (a) and (b) show slopes in the terminal regions (at low frequencies) averaged over all the temperatures (circles 180 °C, upper triangles 160 °C, lower triangles 140 °C, and squares 130 °C). [Color figure can be viewed in the online issue, which is available at wileyonlinelibrary.com.]

The η_0 decreased with increasing temperature and increasing OPE concentration, which was consistent with a plasticization effect of OPE. The significant viscosity decrease might allow little to no change in the processing condition of PE nanocomposites compared to neat PE. Specifically, a substantial amount of nanofillers are needed to induce percolation within the nonpolar PE matrix.[47] At high filler loadings, viscosity increases several orders of magnitude and may cause processing issues. The inclusion of OPE in PE can be used to tune the viscosity of PE nanocomposites. More importantly, the shear thinning behavior of PE remains unperturbed by the incorporation of OPE in PE.

The zero shear viscosity, η_0 changed with OPE loading in the blends at two experimental temperatures tested, i.e., 180 °C and 130 °C [Figure 9(b)]. Small increase in η_0 values (~70%) with a 50 °C change in temperature from 180 to 130 °C indicated

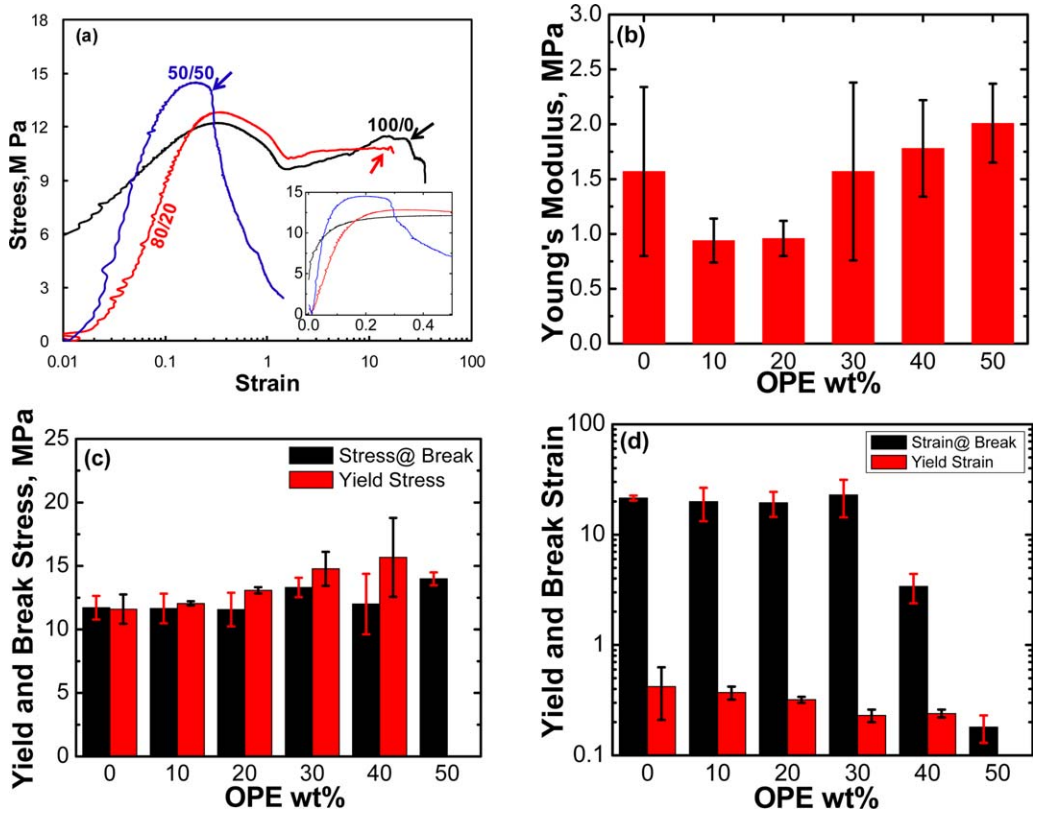

Figure 11. Mechanical properties of PE/OPE blends: (a) Stress−Strain behavior, (b) Young's modulus, (c) yield and break stress, and (d) yield and break strains. Arrows in stress−strain data indicate the break points. The inset in (a) shows stress−strain data on a linear scale. [Color figure can be viewed in the online issue, which is available at wileyonlinelibrary.com.]

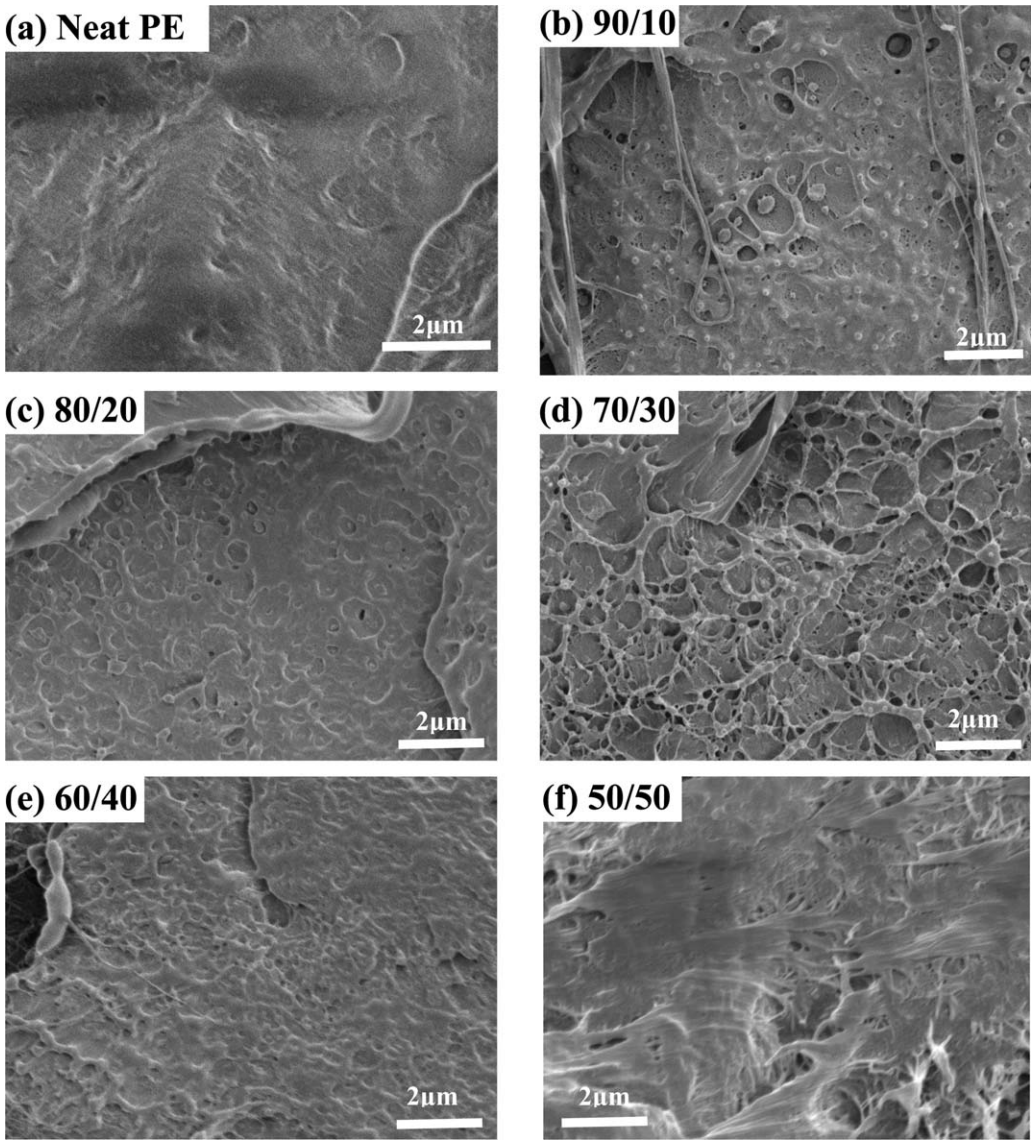

Figure 12. SEM micro-images of PE/OPE blends.

temperature insensitivity of the blends within the accessible temperature range. A linear relationship between log-η_0 and OPE wt % [Figure 9(b)] also showed the melt miscibility of OPE in PE.[11,12,48,49]

It is worth mentioning that the morphology of miscible blends is also considered as a function of viscosity ratio and capillary number.[50] Since, the viscosity of OPE at 145 °C (~0.02 Pa-s, from Arrhenius relation), the viscosity ratio ($p = \eta_d/\eta_m$, where η_d is the viscosity of dispersed phase, and η_m is the viscosity of matrix) becomes extremely low ($p \sim 2 \times 10^{-6}$). At such low viscosity ratios ($p \ll 1$), the droplet diameter essentially remains unchanged, and will have no effect on the blend morphology and droplet break-up processes.[50–52] In addition, very low p has been shown to require a longer mixing time (~30–60 min) to form a consolidated polymer morphology.[53] However, above 60 min, miscible blends of any low viscosity ratio ($p \sim 10^{-6}$) should produce a stable morphology, which also applies in this study (mixing time ~ 120 min).

Time-temperature superposition (TTS) provided master curves for G', G'' for the linear viscoelastic response of the nanocomposites [Figure 10(a–c)]. The validity of TTS was tested by plotting dynamic moduli according to Han's proposed method,[54] which showed only minor fluctuations in the master curves of the blends. The Han's plot and individual $G' \sim f$ master curves are provided in the supporting information. Due to the limitations of experimentally accessible temperatures and temperature insensitivity of blends, the TTS could not be extrapolated over more than 200 s^{-1} frequency. Therefore, the viscoelastic data had been shifted horizontally only. The calculated horizontal shift factor, a_T from the best fit was also plotted versus temperature, and is provided in the supporting information.

No G', G'' plateau was observed within the experimental range. In the low frequency region, G' and G'' were expected to show Maxwell behavior ($G' \sim f^2$, $G'' \sim f^1$). However, neat PE exhibited an un-relaxed behavior at low frequencies ($G' \sim f^{1.1}$), which was observed in similar high molecular weight PE melts.[27,55] The low

frequency slope increased from $G' \sim f^{1.1}$ for neat PE to $G' \sim f^{1.7}$ for 50/50 blend, which approached the relaxed Maxwell behavior attributed to the plasticization effect of OPE. Similarly, at low frequencies, neat PE exhibited $G'' \sim f^{0.8}$ behavior which increased to $G'' \sim f^{1}$ for 50/50 blends, which was an indication of formation of the relaxed chains compare to the neat PE. Furthermore, the formation of relaxed polymer chains with increasing OPE concentration was more evident in the master curves of δ over the reduced frequencies (see supporting information). The delta values increased as OPE concentration increased, approaching $\delta \sim 90°$ for the completely relaxed chains.

In the high frequency regions, PE showed $G' \sim f^{0.5}$, $G'' \sim f^{0.3}$ behavior that changes to $G' \sim f^{0.8}$, $G'' \sim f^{0.7}$ for the 50/50 blend. In the glassy (high frequency) region, PE showed a Rouse longest relaxation time with a general expression $G' \sim f^{0.5}$.[56] Thus, slopes near 0.5 for G' in the high frequency region indicated Rouse dynamics. Increase in high frequency slope, further indicated that the chains did not respond as glassy chains in high frequency region, which confirms the existence of rubbery chains in that region.

Mechanical Properties

Another important factor that determines the practical applications of new polymeric materials is their mechanical performance. Among mechanical properties, tensile properties are considered more important in the initial design of new polymers. The inclusion of OPE reduced the strain at break for the blends [Figure 11(a)]. In agreement with SAXS (Figure 6), the decrease in blends' L_p led to the formation of high Young's modulus materials. The fraction of OPE that decreased the melting point (see thermal analysis discussion earlier) also induced plasticization. The plasticization effect of OPE was quantified by a decrease in Young's modulus from 1.6 MPa for neat PE to 0.94 MPa for 90/10 blends. Further inclusion of OPE chains increased the Young modulus from 0.94 MPa for 90/10 blend to 2.0 for 50/50 blend (~210% increase), which is a direct evidence of the reduced blend elasticity [Figure 11(b)] in agreement with the decreased long period spacing (Figure 6). The change in L_p is also known to influence the elongation at break and yielding strain. A direct consequence of the decreased L_p also resulted in decreasing the elongation at break from 21.5 for PE to 0.18 for 50/50 blends [Figure 11(d)].[57,58] The yield stress [Figure 11(c)] increased from 12 MPa for PE to 16 MPa for 60/40 blends (~74% increase) whereas the yield strain decreased ~90% for 60/40 blends [Figure 11(d)]. In conclusion, OPE in PE decreased the elongation to break for the blends and increased the Young's modulus, consistent with the findings from scattering and thermal analysis.

SEM Morphology

The cryo-fractured surface morphology of neat PE shows a smooth surface upon fracture, which is expected for PE[59] [Figure 12(a)]. When OPE is added into PE and the sample is fractured, some fibrous structures appear to be pulled out from the fractured surfaces [Figure 12(b)]. Denser fibers are observed for 80/20 [see Figure 12(c)] and 60/40 [Figure 12(e)]. However, 70/30 composition shows a distinct morphology, i.e., more abundant fibrous elements [Figure 12(d)]. At this time, we do not have a specific explanation for this behavior, but the unique morphology might account for the higher elongation in the 70/30 blend compared with 90/10 or 80/20 blends. However, the scattering results also indicate this peculiar behavior with 70/30 composition. On the other hand, the 60/40 blends show smooth surface, which is consistent with the reduced viscosity. The 50/50 blend represents a similar surface to the 60/40 blend, but due to the even lower viscosity of that composition, some larger fibers appear after cryo-fracturing.

CONCLUSIONS

A new type of PE/OPE blends has been prepared and the molten and solid state properties of the blends are evaluated at different OPE content. All blends exhibited a negative Flory-Huggins interaction parameter indicating miscibility between PE and OPE that decrease with increasing OPE loading. Increasing OPE concentration in the PE/OPE blends from 0 to 50 wt % decreases the melt temperature from 123 °C to 119 °C and also reduces the thermal stability. The SAXS analysis revealed that the OPE resides inside PE lamellae, and the lamellar thickness decreases with increasing OPE inclusion, leading to increased brittleness that is also confirmed by the increase in modulus and decrease in the strain at break.

Time-temperature superposition master curves showed the formation of relaxed polymer chains with increasing OPE loading and the blends exhibited positive deviation from the Rouse dynamics at higher frequencies. Moreover, incorporation of OPE reduced the zero shear viscosity of the blends suggesting that OPE can also be incorporated as a processing aid. The fractured surface morphology revealed interesting results exhibiting smooth surface of blends with increasing OPE loadings, which is in agreement with the viscosity reduction in blends. In addition, this type of blends with controlled viscosity can also be used to create PE nanocomposites with high filler loadings and can still be processed on neat PE processing conditions. This topic will be the subject of a future manuscript.

ACKNOWLEDGMENTS

This project was supported by The Petroleum Institute, Abu Dhabi through the Cooperative Research Partnership with Colorado School of Mines. The U.S. Army Research Office (DURIP Grant No.W911NF-11-1-0306) is also acknowledged for partial financial support. The authors would also like to thank Prof. John Dorgan for use of his lab facilities, Tara Pandey and Soenke Seifert for assisting in SAXS experiments. Marcus Oils and Chemicals (Texas) are acknowledged for supplying the OPE. The use of the Advanced Photon Source, an office of Science User facility operated for the U.S. Department of Energy (D.O.E.) Office of Science by Argonne National Laboratory was supported by the U.S. DOE under Contract No. DE-AC02-06CH11357.

REFERENCES

1. Utracki, L. A.; Wilkie, C. A. Polymer Blends Handbook; Springer: Netherlands, **2014**; Chapter 1, pp 1–122.
2. Plochocki, A. P. In Polymer Blends; Paul, D.; Newman, S. Eds.; Academic Press: New York, **1978**; Vol. *2*, Chapter 21, pp 319–368.

3. Soontaranum, W.; Higgins, J.; Papathanasiou, T. *J. Non-Newtonian Fluid Mech.* **1996**, *67*, 191.
4. Van Puyvelde, P.; Moldenaers, P. *Rheol. Rev.* **2005**, 101.
5. Wagner, E.; Robeson, L. *Rubber Chem. Technol.* **1970**, *43*, 1129.
6. Cancio, L. V.; Miller, G. W.; Wu, P.-C. U.S. Pat. 4,284,671 A (**1981**).
7. Percec, E. S.; Melamud, L.; Coffey, G. P. U.S. Pat. 5,084,352 A (**1992**).
8. Heuschen, J.; Vion, J.; Jerome, R.; Teyssie, P. *Polymer* **1990**, *31*, 1473.
9. Nishi, T.; Wang, T. *Macromolecules* **1975**, *8*, 909.
10. Vleminckx, G.; Bose, S.; Leys, J.; Vermant, J.; Wubbenhorst, M.; Abdala, A. A.; Macosko, C.; Moldenaers, P. *ACS Appl. Mater. Interfaces* **2011**, *3*, 3172.
11. Hameed, T.; Hussein, I. A. *Polymer* **2002**, *43*, 6911.
12. Utracki, L.; Schlund, B. *Polym. Eng. Sci.* **1987**, *27*, 1512.
13. Hussein, I. A. *Polym. Int.* **2005**, *54*, 1330.
14. Moly, K.; Radusch, H.; Androsh, R.; Bhagawan, S.; Thomas, S. *Eur. Polym. J.* **2005**, *41*, 1410.
15. Gonsalves, K.; Patel, S.; Trivedi, D. *J. Appl. Polym. Sci.* **1992**, *45*, 217.
16. Naqvi, M. K.; Choudhary, M. S. *J. Macromol. Sci. Part C: Polym. Rev.* **1996**, *36*, 601.
17. Kim, H.; Kobayashi, S.; AbdurRahim, M. A.; Zhang, M. J.; Khusainova, A.; Hillmyer, M. A.; Abdala, A. A.; Macosko, C. W. *Polymer* **2011**, *52*, 1837.
18. Guruvenket, S.; Rao, G. M.; Komath, M.; Raichur, A. M. *Appl. Surface Sci.* **2004**, *236*, 278.
19. Schuster, L.; Hettche, A.; Liedy, W.; Weiss, S.; Ehemann, L. U.S. Pat. 5,064,908 A (**1991**).
20. Chen, C.; Wesson, R.; Collier, J.; Lo, Y. *J. Appl. Polym. Sci.* **1995**, *58*, 1107.
21. Weiland, M.; Daro, A.; David, C. *Polym. Degrad. Stabil.* **1995**, *48*, 275.
22. Iring, M. *Prog. Polym. Sci.* **1990**, *15*, 217.
23. Iwata, H.; Kishida, A.; Suzuki, M.; Hata, Y.; Ikada, Y. *J. Polym. Sci. Part A: Polym. Chem.* **1988**, *26*, 3309.
24. Rugg, F. M.; Smith, J. J.; Bacon, R. C. *J. Polym. Sci.* **1954**, *13*, 535.
25. Durmuş, A.; Woo, M.; Kaşgöz, A.; Macosko, C. W.; Tsapatsis, M. *Eur. Polym. J.* **2007**, *43*, 3737.
26. Gugumus, F. *Polym. Degrad. Stabil.* **2002**, *76*, 329.
27. Durmus, A.; Kasgoz, A.; Macosko, C. W. *Polymer* **2007**, *48*, 4492.
28. Vandiver, M. A.; Caire, B. R.; Poskin, Z.; Li, Y.; Seifert, S.; Knauss, D. M.; Herring, A. M.; Liberatore, M. W. *J. Appl. Polym. Sci.* **2015**; *132*, 41596.
29. Liu, Y.; Wang, J.; Yang, Y.; Brenner, T. M.; Seifert, S.; Yan, Y.; Liberatore, M. W.; Herring, A. M. *J. Phys. Chem. C* **2014**, *118*, 15136.
30. Chan, M.; Allara, D. *J. Colloid Interface Sci.* **1974**, *47*, 697.
31. Krupa, I.; Luyt, A. *Polym. Degrad. Stabil.* **2000**, *70*, 111.
32. Mandelkern, L.; Fatou, J.; Denison, R.; Justin, J. *J. Polym. Sci. Part B: Polym. Lett.* **1965**, *3*, 803.
33. Hoffman, J. D.; Weeks, J. J. *J. Chem. Phys.* **1965**, *42*, 4301.
34. Silva, M. E. S.; Mano, V.; Pacheco, R. R.; Freitas, R. F. *J. Mod. Phys.* **2013**, 4, 45.
35. Zhang, L.; Goh, S.; Lee, S.; Hee, G. *Polymer* **2000**, *41*, 1429.
36. Flory, P. J. Principles of Polymer Chemistry; Cornell University Press: New York, **1953**.
37. Sperling, L. H. Introduction to Physical Polymer Science; Wiley: New Jersey, **2006**; Chapter 6, pp 239–323.
38. Ruehle, D. A.; Perbix, C.; Castañeda, M.; Dorgan, J. R.; Mittal, V.; Halley, P.; Martin, D. *Polymer* **2013**, *54*, 6961.
39. Rostami, S. *Eur. Polym. J.* **2000**, *36*, 2285.
40. Painter, P. C.; Shenoy, S. L.; Bhagwagar, D. E.; Fishburn, J.; Coleman, M. M. *Macromolecules* **1991**, *24*, 5623.
41. Glatter, O.; Kratky, O. Small Angle X-ray Scattering; Academic Press: New York, **1982**.
42. Beaucage, G. *J. Appl. Crystallogr.* **1996**, *29*, 134.
43. Jackson, C.; Bauer, B.; Nakatani, A.; Barnes, J. *Chem. Mater.* **1996**, *8*, 727.
44. Canetti, M.; Bertini, F. *Eur. Polym. J.* **2010**, *46*, 270.
45. Rambo, R. P.; Tainer, J. A. *Biopolymers* **2011**, *95*, 559.
46. Cross, M. M. *J. Colloid Sci.* **1965**, *20*, 417.
47. El Achaby, M.; Arrakhiz, F. E.; Vaudreuil, S.; el Kacem Qaiss, A.; Bousmina, M.; Fassi-Fehri, O. *Polym. Compos.* **2012**, *33*, 733.
48. Liu, C.; Wang, J.; He, J. *Polymer* **2002**, *43*, 3811.
49. Kyu, T.; Hu, S. R.; Stein, R. S. *J. Polym. Sci. Part B: Polym. Phys.* **1987**, *25*, 89.
50. Tucker III, C. L.; Moldenaers, P. *Annu. Rev. Fluid Mech.* **2002**, *34*, 177.
51. GRACE†, H. P. *Chem. Eng. Commun.* **1982**, *14*, 225.
52. Everaert, V.; Aerts, L.; Groeninckx, G. *Polymer* **1999**, *40*, 6627.
53. Burch, H. E.; Scott, C. E. *Polymer* **2001**, *42*, 7313.
54. Han, C. D.; Chuang, H. K. *J. Appl. Polym. Sci.* **1985**, *30*, 4431.
55. Meissner, J. *Pure Appl. Chem.* **1975**, *42*, 551.
56. Osaki, K.; Inoue, T.; Uematsu, T.; Yamashita, Y. *J. Polym. Sci. Part B: Polym. Phys.* **2001**, *39*, 1704.
57. Neppalli, R.; Marega, C.; Marigo, A.; Bajgai, M. P.; Kim, H. Y.; Causin, V. *Eur. Polym. J.* **2010**, *46*, 968.
58. Pukánszky, B.; Mudra, I.; Staniek, P. *J. Vinyl Add. Technol.* **1997**, *3*, 53.
59. Jeong, S.; Kim, D.; Seo, J. *Prog. Org. Coat.* **2015**, *85*, 76.